

## Optical Insight Into Riverine Influences on Dissolved and Particulate Organic Carbon in a Coastal Arctic Lagoon System

L. Catipovic<sup>1,2</sup> , K. Longnecker<sup>1</sup>, S. R. Okkonen<sup>3</sup> , D. Koestner<sup>4</sup> , and S. R. Laney<sup>1</sup> 

<sup>1</sup>Woods Hole Oceanographic Institution, Woods Hole, MA, USA, <sup>2</sup>MIT-WHOI Joint Program in Oceanography, Woods Hole, MA, USA, <sup>3</sup>University of Alaska Fairbanks, Fairbanks, AK, USA, <sup>4</sup>University of Bergen, Bergen, Norway

### Key Points:

- Absorption, fluorescence, and spectral slope are conditionally accurate optical proxies for dissolved organic carbon in nearshore coastal Arctic waters
- River discharge appears to be the primary driver of spatial distributions of organic matter in Stefansson Sound during the open water season
- The backscattering coefficient can serve as a conditional proxy for particulate organic carbon concentration in nearshore coastal Arctic waters

### Correspondence to:

L. Catipovic,  
lcatipovic@whoi.edu

### Citation:

Catipovic, L., Longnecker, K., Okkonen, S. R., Koestner, D., & Laney, S. R. (2023). Optical insight into riverine influences on dissolved and particulate organic carbon in a coastal Arctic lagoon system. *Journal of Geophysical Research: Oceans*, 128, e2022JC019453. <https://doi.org/10.1029/2022JC019453>

Received 2 NOV 2022  
Accepted 30 MAR 2023

**Abstract** Arctic coastal margins receive organic material input from rivers, melted sea ice, and coastal erosion, phenomena that are all undergoing changes related to global climate. The optical properties of coastal Arctic waters contain information on this organic material, and we examined three optical properties of seawater (absorption, backscatter, and fluorescence) for their relationships to variability in dissolved and particulate organic carbon (DOC and POC) in Stefansson Sound, Alaska, a coastal Arctic embayment. During open water periods in 2018 and 2019, DOC was inversely correlated with salinity ( $r^2 = 0.97$ ) and positively correlated with dissolved organic matter fluorescence (fDOM;  $r^2 = 0.67$ ). DOC showed strong correlation with the nonparticulate absorption coefficient at 440 nm ( $a_g(440)$ ) only in 2018 ( $r^2 = 0.95$ ). The vertical structure of fDOM in Stefansson Sound aligned with density profiles more strongly in 2018 than in 2019, and higher levels of fDOM,  $a_g(440)$ , and backscatter seen near the bottom in 2019 suggest wind-driven mixing and/or bottom resuspension events. In both years, DOC correlated strongly with the spectral slope of the absorption coefficient between 412 and 550 nm ( $r^2 = 0.70$ ), and POC was well correlated with spectral backscattering at 470, 532, and 660 nm ( $r^2 = 0.90, 0.71, \text{ and } 0.59$ ). These interannual differences in the spatial and vertical distributions of DOC and POC, and their respective correlations with optical proxies, likely reflect regional climatological factors such as precipitation over the adjacent watersheds, wind patterns, and residual sea ice in late summer.

**Plain Language Summary** Arctic coastal waters are experiencing drastic changes in response to changing global climate, many of which can affect the biology and biogeochemistry of these waters in the ice-free summer months. Optical methods are potentially valuable for measuring changes in the amount of particulate and dissolved organic carbon in seawater. To study the biogeochemistry of organic carbon in the coastal Arctic using optical properties, we must first understand their relationships in these optically complex waters. This study examines these relationships within a 2-year study in Stefansson Sound, a coastal embayment along the Alaskan Arctic Ocean. We found that across 2 years with differing residual sea ice in summer and rainfall trends in the adjacent watersheds, some optical properties can be useful proxies for dissolved and particulate carbon in seawater. For these two specific years, we observed that the amount of dissolved organic carbon found in this region is likely related to the precipitation over the adjacent watersheds, which increases the river flow and delivery of terrestrial organic carbon into these coastal waters.

## 1. Introduction

The coastal Arctic Ocean experiences seasonal landfast ice cover, intermittent freshwater inputs from coastal rivers, and strong winds: all environmental factors that are affected by a changing global climate. These climate-driven changes in turn can alter the physical environment of these coastal waters, for example, via warming temperatures that increase sediment and organic matter inputs via rivers, groundwater discharge, and coastal erosion (Connolly et al., 2020; Jones et al., 2009; McClelland et al., 2016). The consequences to biogeochemical processes can be seen when such increases in riverine supply provide more bioavailable organic material to coastal ocean ecosystems that then is respired microbially to produce greater amounts of carbon dioxide (Holmes et al., 2008). Such climatological changes can also have indirect effects on biogeochemical cycling, for example, by increasing particle loads that reduce light transmission through the water column and limit photosynthesis (Klein et al., 2021).

Stefansson Sound is one of the many estuaries, bays, and lagoons along the Alaskan Arctic coastal margin that receive intermittent freshwater input from rivers. Stefansson Sound is fed by the Sagavanirktok and Kuparuk

© 2023. The Authors.

This is an open access article under the terms of the [Creative Commons Attribution-NonCommercial-NoDerivs License](#), which permits use and distribution in any medium, provided the original work is properly cited, the use is non-commercial and no modifications or adaptations are made.

Rivers and is partially enclosed by barrier islands 10–15 km offshore. The sources and fates of organic matter in these coastal Arctic embayments are poorly understood, as are the areal and vertical distributions of organic matter and any interannual variability that is driven by large-scale climatological trends. These coastal systems are further complicated by the seasonal presence of sea ice, annual events such as the spring freshet, and intermittency in discharge of any local rivers that deliver organic matter into the coastal margin (Matsuoka et al., 2012; Stedmon et al., 2011). The two largest rivers that feed Stefansson Sound (the Sagavanirktok and the Kuparuk) drain watersheds overlain by differing land types, with the Sagavanirktok watershed encompassing a mixture of mountainous and tundra regions, while the Kuparuk encompasses primarily tundra (McClelland et al., 2014). Such differences in watershed geomorphology, and also the slope of these catchments, have been shown to relate to organic matter concentration in fluvial discharge (Connolly et al., 2018). Melting snow cover and thawing tundra in coastal Alaskan watersheds begin in late May, resulting in a rapid increase in fluvial discharge that can account for more than half of the freshwater delivered annually by rivers into the Alaskan coastal margin (McClelland et al., 2014).

In addition to riverine sources, transported sea ice is another mechanism that delivers freshwater and organic matter to the coastal Alaskan Arctic. With a warming Arctic, ice that is transported from the Canadian Basin through the Beaufort Sea is increasingly composed of younger, often first-year ice (Howell et al., 2016) that is more likely to break off from the pack and drift shoreward. When this ice eventually melts in the coastal margins, it provides a new source of fresh water and organic matter to the surface ocean (Underwood et al., 2019). Organic material in sea ice is derived from three primary sources: particles entrained into the ice during freezing, solutes excluded from seawater during freezing and retained in brines, and organic material associated with ice biota and their exudates (Belzile et al., 2000).

The complex intricacies of these coastal estuaries require a systems-level approach to adequately describe the spatial characteristics of organic and optical properties. Several optical properties of seawater provide insight into the distributions and characteristics of any organic carbon it contains, even in optically complex coastal waters (Osburn et al., 2016; Reynolds et al., 2016). Three particular optical properties of seawater have been shown to positively correlate with the concentration of organic matter: the fluorescence of dissolved organic matter (fDOM), the spectral absorption coefficient of the dissolved fraction ( $a_g(\lambda)$ ), and the optical backscattering coefficient ( $b_b(\lambda)$ ). Optical properties of seawater moreover serve as indicators of its source and composition (Gonçalves-Araujo et al., 2016; Matsuoka et al., 2011; Reynolds et al., 2016). Used as proxies, these optical properties are well suited for studying biogeochemical parameters such as organic carbon distribution, source, concentration, and quality, at higher spatial and temporal scales than can be achieved via discrete sampling (Chang & Dickey, 2001). Instruments that measure optical backscatter and fluorescence are being increasingly used in autonomous systems to obtain time series to examine seasonal and annual aspects of coastal Arctic biogeochemistry (Laney & Okkonen, 2022), and such optical data have significant potential for improving our understanding of carbon cycle dynamics in the coastal Arctic. However, robust use of these observations requires that relationships between these optical proxies and analytical measurements of organic matter concentration be better understood.

We conducted a 2-year field study in 2018 and 2019 to examine relationships between organic carbon and fluorescence, absorption, and backscatter in optically complex coastal Arctic waters, using Stefansson Sound as a model system. We describe relationships between optical proxies and analytically measured dissolved organic carbon (DOC) and particulate organic carbon (POC) concentrations and assess their efficacy for estimating characteristics associated with source and composition. We next examined vertical profiles of absorption, fDOM, and backscatter to examine the areal and vertical distribution of organic matter in Stefansson Sound and how those distributions vary between our two study years. We then examined oceanographic factors that might account for various differences we observed between years in these optical relationships.

## 2. Methods

### 2.1. Study Area

Distributions of DOC and POC, along with the absorption coefficient of dissolved matter at 440 nm ( $a_g(440)$ ), total backscattering coefficients at 470, 532, and 660 nm ( $b_b(470)$ ,  $b_b(532)$ , and  $b_b(660)$ ), fDOM, temperature, and salinity were measured in Stefansson Sound in late summer of 2018 (6–10 September) and 2019 (9–13

August). Stefansson Sound is a shallow lagoon system, partially enclosed by barrier islands along the Beaufort Shelf, that receives input from two principal rivers with deltas spaced  $\sim 30$  km apart: the Sagavanirktok River (14,300 km<sup>2</sup> drainage area) and the Kuparuk River (8,100 km<sup>2</sup> drainage area). Several smaller rivers also provide freshwater to Stefansson Sound, including the Shaviovik River (4,030 km<sup>2</sup> drainage area) and the Kadleroshilik River (1,290 km<sup>2</sup> drainage area). These rivers all drain tundra watersheds but the Sagavanirktok and Shaviovik watersheds also include mountainous regions of the Brooks Range at their headwaters south of the coast.

Samples were collected at locations within and around Stefansson Sound, arranged to encompass the areas receiving input from the mouths of the two principal rivers (Figure 1). In 2018, sampling was restricted to inshore locations to respect the local whaling operations. In 2019, sampling covered a similar inshore region but included three stations not visited in 2018: one at the mouth of the Kuparuk River delta (KO), one just outside the barrier islands north of the mouth of the Sagavanirktok River (S2), and one at the shelf break  $\sim 60$  km offshore directly north of the mouth of the Kuparuk River (UPE80). These stations were chosen to represent riverine and oceanic endmembers, respectively.

## 2.2. Discrete Sampling of DOC and POC

Samples for dissolved and particulate analysis were collected from the depths listed in Table 1 using 5 L Niskin bottles. The bottom depth at the Kuparuk River mouth was  $< 2$  m and thus only surface samples were taken at that location (station KO in Figure 1). Samples for DOC were filtered through combusted Whatman 47 mm diameter glass fiber filters (GF/F; nominal pore size 0.7  $\mu\text{m}$ ) and then acidified to pH 2 with 12 M HCl and stored at 4°C until processed at the Woods Hole Oceanographic Institution on a Shimadzu TOC-V<sub>CSH</sub> total organic carbon analyzer. Reported DOC data are the average of triplicate samples taken at each depth except for at N1 in 2018 and KO in 2019 from which there are only two replicates. Across all samples, the coefficients of variation of replicates were on average 1.6% in 2018 and 3.9% in 2019. Measurements were made using potassium hydrogen phthalate as a standard solution. DOC concentration was determined by subtracting the instrument blank area from the average peak area and dividing by the slope of the standard curve. Comparisons to low carbon water and deep-sea reference water provided by Prof. D. Hansell (University of Miami) were made daily.

For the analysis of POC concentration, approximately 100–1,400 mL of seawater was filtered through 25 mm diameter GF/F filters (nominal pore size 0.7  $\mu\text{m}$ ) at low vacuum ( $< 120$  mm Hg) using precombusted filters. Filters with retained particles were dried in a small oven at  $\sim 55^\circ\text{C}$  and stored for laboratory-based analysis. Elemental carbon analysis of POC filters was performed at the University of California Santa Barbara Marine Science Institute Analytical Laboratory following standard methodology (Parsons et al., 1984). Blank filters were prepared utilizing approximately 50 mL of GF/F (47 mm, nominal pore size 0.7  $\mu\text{m}$ ) filtered seawater collected from several stations to adjust POC estimates for adsorption of DOC onto the filters as well as other sources of contamination (Novak et al., 2018). These corrections resulted in an average reduction of 11% for POC. Duplicate filters were collected, and results were averaged in duplicate (when possible) to determine a final estimate of POC at each station's sampling depths. Coefficients of variation between replicates of POC were on average 7%.

## 2.3. Watershed and River Characteristics

Volumetric discharges were provided by USGS stream gauges on the Kuparuk River (USGS 15896000, located 9 km upstream from the river mouth) and the Sagavanirktok River (USGS 15908000, located roughly 90 km upstream from the river mouth). Volumetric discharge from the stream gauges is reported every 15 min. Precipitation data from the University of Alaska at Fairbanks' Toolik field station (68.63°N, 149.60°W), 200 km south of the coast, were used representatively as a metric of rainfall over the watersheds of the rivers. These data were collected using a tipping bucket rain gauge (Texas Electronics TE525WS; EDCT, 2020; Youcha et al., 2015). We report these precipitation data here as a 24-hr running mean. Cumulative precipitation reported in the week prior to each sampling period was estimated by calculating the area under the running mean using the trapezoidal method.

## 2.4. Hydrographic and Optical Properties of Vertical Profiles

Water column structure was measured at each station using a custom profiling package. The instruments on this package were separated at maximum by  $\sim 0.5$  m and vertical offsets between sensors were corrected for during

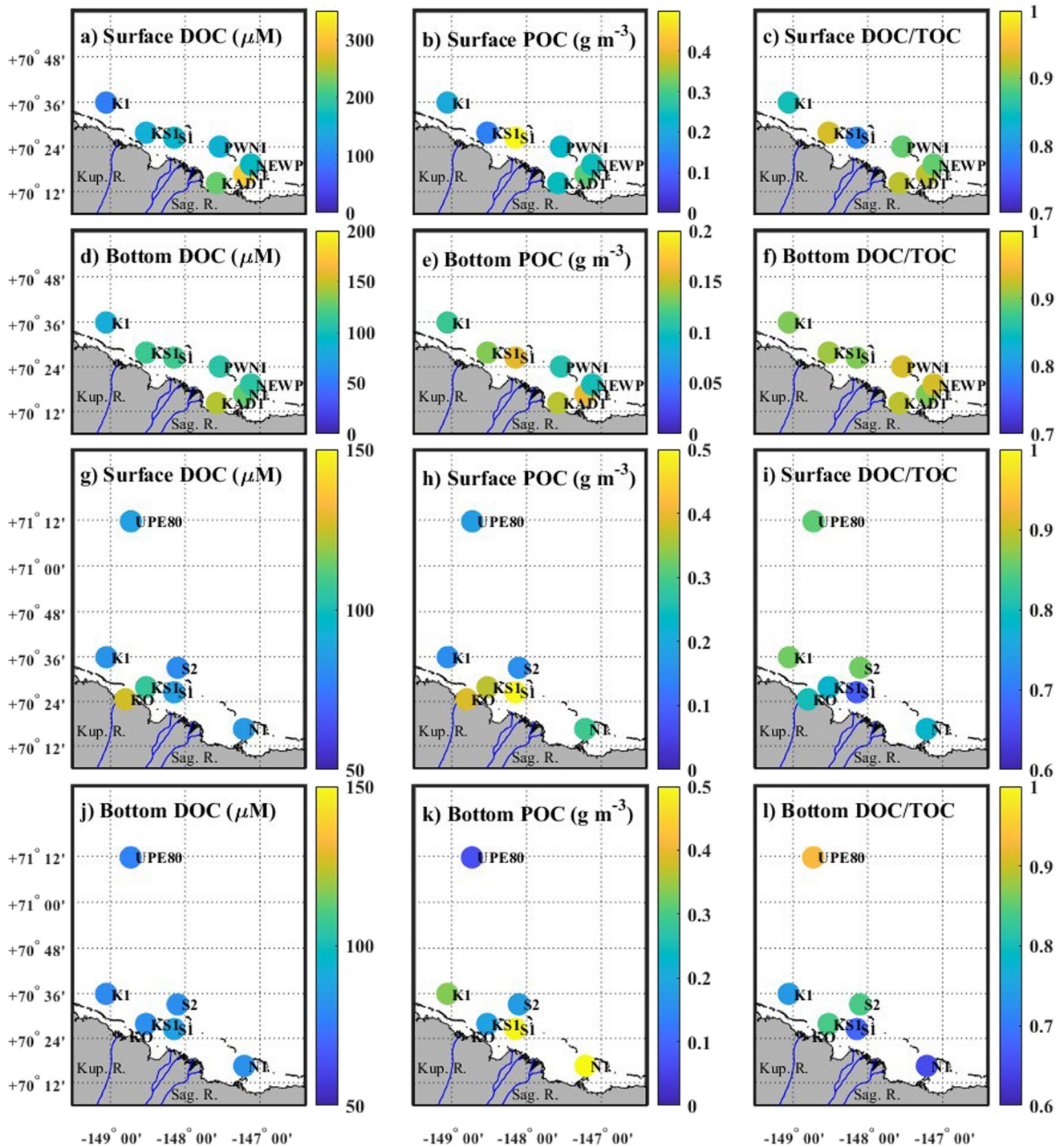


**Figure 1.** Sample locations for the field season of September 2018 (a–f) and August 2019 (g–l). Color-correlated markers indicate dissolved organic carbon (DOC), particulate organic carbon (POC), and fraction dissolved (DOC/TOC, where TOC is DOC + POC) at the surface and the bottom.

postprocessing, so as to align all measurements made during profiling. The suite of sensors included hydrographic and optical instruments: a conductivity, temperature, and depth meter (SBE-49 FastCAT), a spectral absorption and attenuation meter (WETLabs ac-s), a three-channel active sensor (WETLabs FLBBOD) which provided measurements of the fDOM, and a three-wavelength volume scattering function sensor (WETLabs VSF3). The VSF3 measures the volume scattering function ( $\beta$ ) at scattering angles of  $100^\circ$ ,  $125^\circ$ , and  $150^\circ$  for light wavelengths of 470, 532, and 660 nm. Backscattering coefficients for each light wavelength were calculated

**Table 1**  
*DOC and POC Concentrations and Fraction Dissolved at the Surface and Bottom From Both Field Seasons*

Station	Property	2018		2019	
		Surface	Bottom	Surface	Bottom
KO	Sample depth	–	–	0.6	–
	DOC	–	–	126 ± 0.8	–
	POC	–	–	0.388 ± 0.011	–
	DOC/TOC	–	–	0.80 ± 0.01	–
K1	Sample depth	1.1	13.6	2.0	17.3
	DOC	92.1 ± 4.1	83.1 ± 1.87	83.0 ± 5.06	79.7 ± 0.99
	POC	0.202 ± 0.005	0.115 ± 0.000	0.156 ± 0.047	0.335 ± 0.013
	DOC/TOC	0.85 ± 0.06	0.90 ± 0.03	0.86 ± 0.09	0.74 ± 0.02
KS1	Sample depth	1.5	6.1	1.5	6.4
	DOC	148 ± 1.34	116 ± 3.30	107 ± 0.73	81.5 ± 7.36
	POC	0.133 ± 0.018	0.134 ± 0.009	0.366 ± 0.045	0.189 ± 0.037
	DOC/TOC	0.93 ± 0.01	0.91 ± 0.04	0.78 ± 0.02	0.84 ± 0.12
S1	Sampled depth	1.1	5.7	1.7	6.5
	DOC	159 ± 4.3	117 ± 0.87	86.9 ± 8.0	87.5 ± 6.02
	POC	0.502 ± 0.024	0.159 ± 0.003	0.509 ± 0.078	0.493 ± 0.065
	DOC/TOC	0.79 ± 0.04	0.90 ± 0.01	0.67 ± 0.12	0.68 ± 0.09
S2	Sample depth	–	–	1.4	17.0
	DOC	–	–	80.1 ± 1.81	81.3 ± 0.98
	POC	–	–	0.158 ± 0.010	0.181 ± 0.032
	DOC/TOC	–	–	0.86 ± 0.03	0.84 ± 0.03
PWNI	Sample depth	1.3	6.2	–	–
	DOC	153 ± 0.76	108 ± 1.43	–	–
	POC	0.234 ± 0.00	0.104 ± 0.00	–	–
	DOC/TOC	0.89 ± 0.01	0.93 ± 0.02	–	–
KAD1	Sample depth	1.1	4.7	–	–
	DOC	223 ± 0.79	145 ± 2.83	–	–
	POC	0.242 ± 0.00	0.146 ± 0.00	–	–
	DOC/TOC	0.92 ± 0.00	0.92 ± 0.03	–	–
NEWP	Sample depth	1.4	6.6	–	–
	DOC	168 ± 1.27	109 ± 0.83	–	–
	POC	0.248 ± 0.001	0.100 ± 0.000	–	–
	DOC/TOC	0.89 ± 0.01	0.93 ± 0.01	–	–
N1	Sample depth	1.3	6.0	1.4	5.2
	DOC	310 ± 4.50	127 ± 1.42	84.8 ± 5.43	82.4 ± 7.14
	POC	0.310 ± 0.026	0.160 ± 0.014	0.291 ± 0.044	0.536 ± 0.072
	DOC/TOC	0.92 ± 0.02	0.90 ± 0.02	0.78 ± 0.08	0.65 ± 0.10
UPE80	Sample depth	–	–	2.3	47.50
	DOC	–	–	87.1 ± 1.50	78.1 ± 1.65

**Table 1**  
*Continued*

Station	Property	2018		2019	
		Surface	Bottom	Surface	Bottom
	POC	–	–	0.181 ± 0.034	0.070 ± 0.016
	DOC/TOC	–	–	0.85 ± 0.02	0.93 ± 0.03

*Note.* DOC is reported in units of micromolar, POC is reported in units of g m<sup>-3</sup>, and the conversion to micromolar takes the form:  $\frac{1 \text{ g C}}{1 \text{ m}^3} \times \frac{1 \text{ e}6 \mu\text{g C}}{1 \text{ g C}} \times \frac{1 \text{ m}^3}{1,000 \text{ L}} \times \frac{1 \mu\text{mol C}}{12.01 \mu\text{g C}} [=] \frac{\mu\text{mol C}}{\text{L}}$ . DOC/TOC ratio is unitless. Reported errors are standard deviation within a triplicate or duplicate set of samples unless the error is zero in which case only one replicate is reported.

following standard methods recommended by the manufacturer. Briefly, the measured  $\beta$  values were converted to polar steradian area, fitted using a third-order polynomial to the new values with an added fourth point ( $\sin(\pi \text{ radians}) = 0$ ), and integrated under the polynomial fit function from  $\pi/2$  to  $\pi$ . This method results in a maximum 1% error when tested against published volume scattering functions (Petzold, 1972). The WETLabs FLBBBCD measures fDOM fluorescence of 460 nm light with an excitation wavelength of 370 nm (370/460 nm), which aligns with the expected fluorescence of terrestrial humic material anticipated to be injected by the rivers into the coastal margin (Ward & Cory, 2015).

To provide information on the optical properties of dissolved constituents in seawater, the package was deployed with a 0.2  $\mu\text{m}$  capsule filter (Whatman POLYCAP AS) placed on the inlet of the ac-s pump. These ac-s data were processed using proprietary software from the vendor and then further corrected for temperature and salinity using algorithms written in MATLAB 2021a (Sullivan et al., 2006). Spectral slopes of absorption between 412 and 550 nm ( $S_{412-550}$ ) were calculated using a single exponential model fit of these corrected spectra. When sampling in the field, the sensor package was allowed to rest for 5 min at the near-surface and near-bottom depths, to allow adequate time to collect a statistically significant number of samples from depths where discrete water samples were retrieved for DOC and POC analysis. Mixed layer depths were determined from the most relevant maximum Brunt-Vaisala frequency peak in each profile. Mixed layer depths were defined as the first peak below the peak associated with the freshwater lens, which was generally found in the upper 2 m of the water column.

## 2.5. Statistical Analyses

Model II geometric mean linear regression analyses were performed to determine the strength of any relationships between various optical proxies and DOC or POC. Regression models were evaluated for accuracy using two common metrics: root mean square deviation (RMSD) and median absolute percent difference (MdAPD). The RMSD assesses model accuracy in absolute units by quantifying the mean of the squared residuals between the observed and the model-predicted values and thus can be susceptible to outliers. The MdAPD is less sensitive to large errors by utilizing the median of the absolute difference between model-predicted and observed values, normalized by observed values, and provides a standard metric for model assessment as a percentage.

## 3. Results

### 3.1. Spatial Distribution of Organic Matter in Stefansson Sound

In 2018, DOC concentrations ranged from 92.1 to 310  $\mu\text{M}$  at the surface and 83.1 to 127  $\mu\text{M}$  near the bottom. In this same year, POC values ranged from 0.133 to 0.502 g m<sup>-3</sup> at the surface and 0.100 to 0.160 g m<sup>-3</sup> near the bottom. In 2019, we observed DOC concentrations ranging from 80.1 to 127  $\mu\text{M}$  at the surface and 78.1 to 87.5  $\mu\text{M}$  near the bottom, and POC values ranging from 0.156 to 0.509 g m<sup>-3</sup> at the surface and 0.070 to 0.536 g m<sup>-3</sup> near the bottom. The fraction of DOC to total organic carbon (DOC/[DOC + POC]) was above 0.85 for all samples in 2018 and ranged from 0.65 to 0.93 in 2019 (Figure 1 and Table 1). In 2018, higher DOC concentrations were observed at the eastern stations (PWNI, N1, NEWP, and KAD1) than at the western stations (K1, KS1, and S1; unpaired  $t$  test,  $p = 0.138$ ), whereas in 2019, DOC concentrations were more uniform across the study area. The difference between surface and bottom DOC concentrations was significantly higher in 2018 than in 2019 (unpaired  $t$  test,  $p < 0.05$ ). In 2019, the DOC concentrations were generally similar to that observed at the offshore UPE80 station, suggesting a high proportional presence of offshore water in the inshore coastal

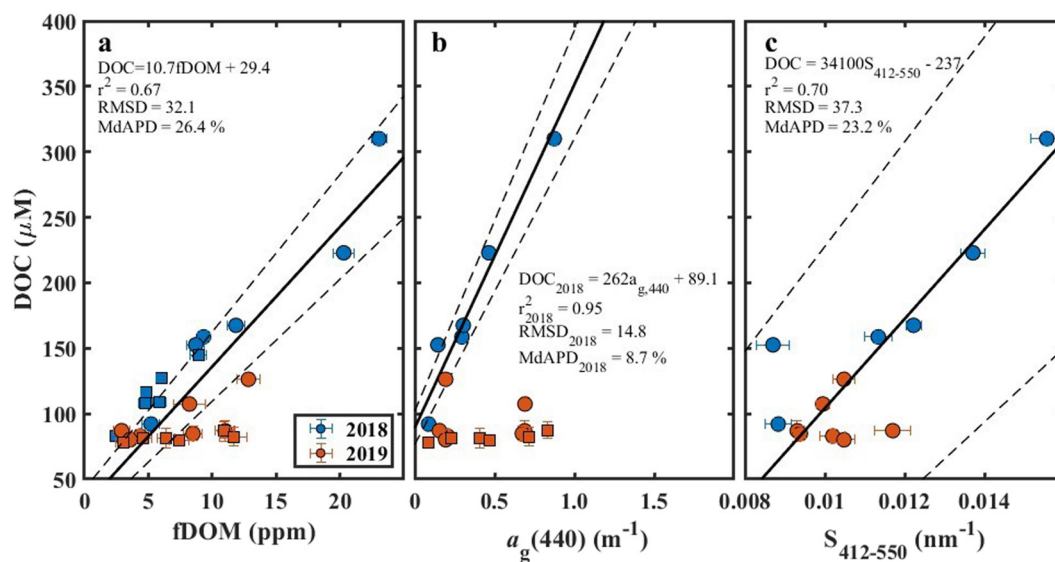


**Figure 2.** Linear regressions between dissolved organic carbon (DOC) and optical variables across both years: (a) fluorescence of dissolved organic matter (fDOM; 370 nm/460 nm), (b)  $a_g(440)$ , and (c)  $S_{412-550}$ . Symbols indicate surface samples (circles) and samples collected below the mixed layer (squares, not included in regressions). Dotted lines indicate  $\pm$ SD.

margin, and a well-mixed water column. Surface POC concentrations were significantly higher than bottom concentrations in 2018 (unpaired  $t$  test,  $p < 0.05$ ), while concentrations measured in 2019 exhibited no significant areal or vertical differences.

### 3.2. Relationships Between Optical Properties and Organic Matter

Over both years, we observed positive correlations between DOC and three optical variables: fDOM,  $a_g(440)$ , and  $S_{412-550}$  (Figure 2). The correlation between fDOM and DOC was strong ( $r^2 = 0.67$ ); however, the strength of the regression is heavily weighted by the 2018 relationship between the two variables ( $r^2 = 0.94$ ), as we observed significantly higher surface DOC concentrations than were seen in 2019 (Table 1; unpaired  $t$  test,  $p < 0.05$ ). The regression was weaker in 2019 ( $r^2 = 0.29$ ) which decreased the overall correlation when considering both years (Figure 2a). The value of the regression model y-intercept suggests that 29.4  $\mu$ M of the DOC pool does not fluoresce at the 370 nm excitation wavelength used by our fluorometer.

The concentration of DOC correlated strongly with  $a_g(440)$  in 2018 ( $r^2 = 0.95$ ) and was uncorrelated in 2019 ( $r^2 < 0.001$ ; Figure 2b). Extrapolating the 2018 regression to the y-intercept suggested that 89.1  $\mu$ M of DOC does not absorb 440 nm light, which is nearly 3 times the concentration that does not fluoresce at 370 nm as stated above. The spectral slope between 412 and 550 nm ( $S_{412-550}$ ) correlated well with DOC concentration across both years ( $r^2 = 0.71$ ) reflecting an increase in DOC with increasing  $S_{412-550}$  (Figure 2c). The negative value at the y-intercept of the regression suggests that there is no concentration of DOC that would be described by a spectral slope of zero between these wavelengths, although the uncertainty bounds of this regression are quite large.

Correlations between POC concentration and all three measured wavelengths of optical backscatter were strong ( $r^2 = 0.90$ ,  $r^2 = 0.71$ , and  $r^2 = 0.59$  for 470, 532, and 660 nm, respectively; Figure 3). The sensor maximum for our instrument was highest when measuring  $b_b(470)$  and lowest when measuring  $b_b(660)$ , resulting in the inclusion of more data points in the POC versus  $b_b(470)$  relationship ( $n = 23$ ) and fewer in the relationships with  $b_b(532)$  and  $b_b(660)$  ( $n = 20$  and  $n = 16$ , respectively).

The regression for POC and  $b_b(532)$  falls within the range reported by other studies representative of mineral-dominated particulate assemblages and of assemblages inclusive of inorganic and organic particulates (Koestner et al., 2021; Reynolds et al., 2016). The regression model derived by Koestner et al. (2021) was determined from POC samples taken from the same cruises in the current study but using a different scattering meter (LISST-VSF, Sequoia Scientific). Additional analysis described in Koestner et al. (2021) revealed that these particulate assemblages were primarily inorganic dominated.

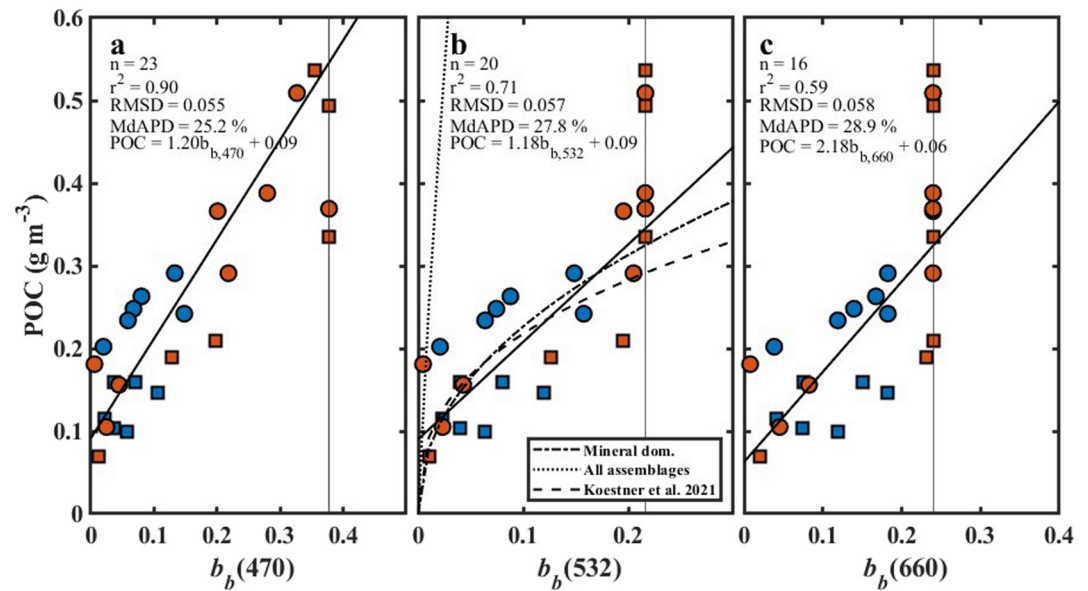


**Figure 3.** Particulate organic carbon (POC) versus backscattering of (a) 470 nm, (b) 532 nm, and (c) 660 nm light. (b) Includes regression lines showing relationships between POC and  $b_b(550)$  in mineral-dominated assemblages and all assemblages from Reynolds et al. (2016), and a relationship between POC and  $b_b(552)$  measured by a LISST-VSF in Stefansson Sound from Koestner et al. (2021). Data lying on the vertical lines in each panel are at sensor maximum and are not included in the regressions. The colors and shapes of the symbols are as described in Figure 2.

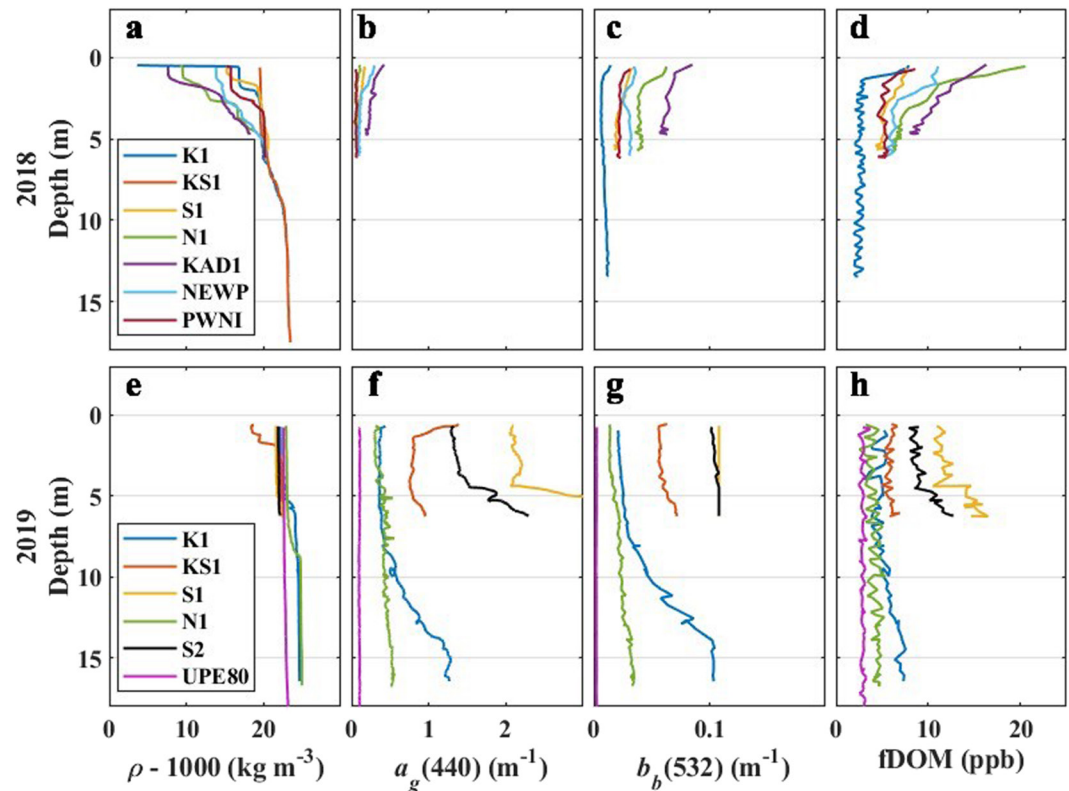


**Figure 4.** 2018 (a–d) and 2019 (e–h) vertical profiles from each station of density of seawater ( $\rho$ ),  $a_g(440)$ ,  $b_b(532)$ , and fluorescence of dissolved organic matter (fDOM). Profiles from UPE80 continue to 47 m of depth with little variation from the values shown at 18 m.

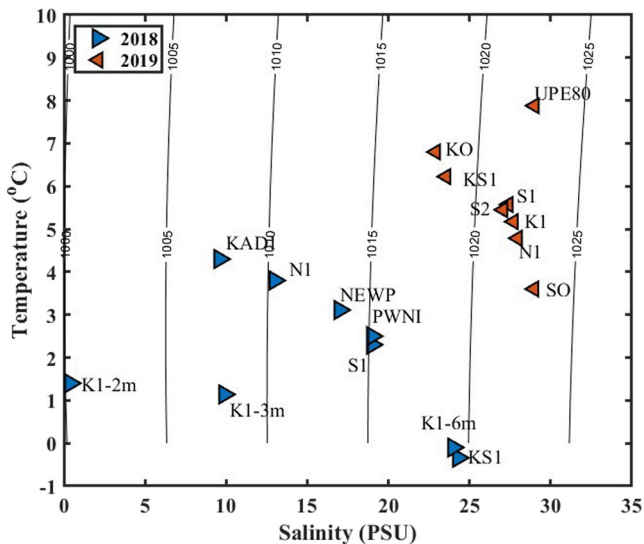


**Figure 5.** Temperature and salinity relationships for all surface samples collected across both field seasons. Lines indicate contours of constant density in units of  $\text{kg m}^{-3}$ . In 2018, station K1 was covered by an ice floe and had multiple strata near the surface.

### 3.3. Physical and Optical Vertical Structure

The vertical character of water column density (Figure 4, left column) in both years indicated a freshwater source to the surface waters. In 2018, density profiles tended to have at least two distinct layers, with weak stratification throughout the water column. This was seen in every station except KS1 which lies west of the Sagavanirktok River. Station K1 also lies west of the Sagavanirktok River but was covered by an ice floe during our 2018 sampling. Profiles at this location showed multiple strata formed by the melting of this ice along with riverine injection of freshwater (Figure 4). The vertical structure measured in 2019 displayed a more well-mixed water column with much higher surface salinities. At the deeper stations (K1, S2, and UPE80), a defined mixed layer was observed over an oceanic layer, but the transition is found much deeper at  $\sim 4$ ,  $\sim 8$ , and  $\sim 19$  m, respectively.

In both years, at least to some extent, the density structure is reflected in the shape of optical profiles. The 2018 optical profiles of  $a_g(440)$ ,  $b_b(532)$ , and fDOM loosely mirror density profiles where each optical proxy showed higher values near the surface than near the bottom (Figure 4). At most stations in 2018, lower density water contained elevated levels of fDOM and  $b_b(532)$  correlating with elevated levels of DOC and POC (Figures 2 and 3), which is expected in water of terrigenous origin. In 2019,  $a_g(440)$ ,  $b_b(532)$ , and fDOM are generally highest near the bottom with constant values near the top and midwater column.

### 3.4. Stefansson Sound: Hydrography, Hydrology, and Wind

We observed clear separation in surface temperature and salinity between both years despite returning to three of the same stations in the second year of our study. In 2018, mean surface salinity across all stations within the coastal margin was 13.9 PSU, while in 2019, mean surface salinity in the same region was significantly higher at 26.8 PSU (unpaired  $t$  test,  $p < 0.05$ ). The mean surface temperature was colder in 2018 compared with 2019 ( $2.3^\circ\text{C}$  vs.  $5.7^\circ\text{C}$ ; unpaired  $t$  test,  $p < 0.05$ ; Figure 5). The salinity of the ambient water covering the shelf has been observed to vary from 20 to 35 PSU annually with fresher values during the summer months when the rivers are running, while water temperatures range from  $-1.6^\circ\text{C}$  to  $-1.8^\circ\text{C}$  during winter (Weingartner & Okkonen, 2001) and increase to as high as  $8^\circ\text{C}$  in this study during August 2019. The separation in temperature–salinity space between the two years is likely attributable to changes in freshwater injection by rivers as well as the presence of sea-ice meltwater in 2018 and interannual differences in wind-driven mixing.

Year-to-year differences in vertical density structures also likely reflect year-to-year differences in river waters discharged into the coastal margin during each year. In the week prior to the 2018 sampling effort, 50% more accumulated precipitation was recorded at Toolik Field station than in the week prior to the 2019 sampling effort. This relative increase in precipitation over the adjacent watershed was reflected by a 66% increase in the cumulative volumetric discharge in the 1–10 September 2018 period over the 4–13 August 2019 period (Figure 6). Moreover, the USGS Sagavanirktok stream gauge near Trans-Alaska Pipeline Pump Station #3 recorded river water temperatures of  $\sim 4^\circ\text{C}$  in 2018 and  $\sim 8^\circ\text{C}$  in 2019 during each respective sample period. This in turn was reflected by cooler and fresher surface waters in the coastal margin in 2018 (Figure 5).

## 4. Discussion

This study explores optical and biogeochemical relationships in Stefansson Sound over two consecutive late-summer open water seasons. We found strong correlations between common optical proxies and analytically measured DOC and POC concentrations despite there being complex differences in the hydrology and hydrography in the coastal margin between the 2 years. Various physical phenomena (e.g., wind velocity, rainfall over the adjacent terrestrial watersheds, and the presence of sea ice) create optical complexity in coastal Arctic waters and in Stefansson Sound particularly. This study examines how these physical properties affect the relationships between optical proxies and organic matter in this model coastal Arctic system.

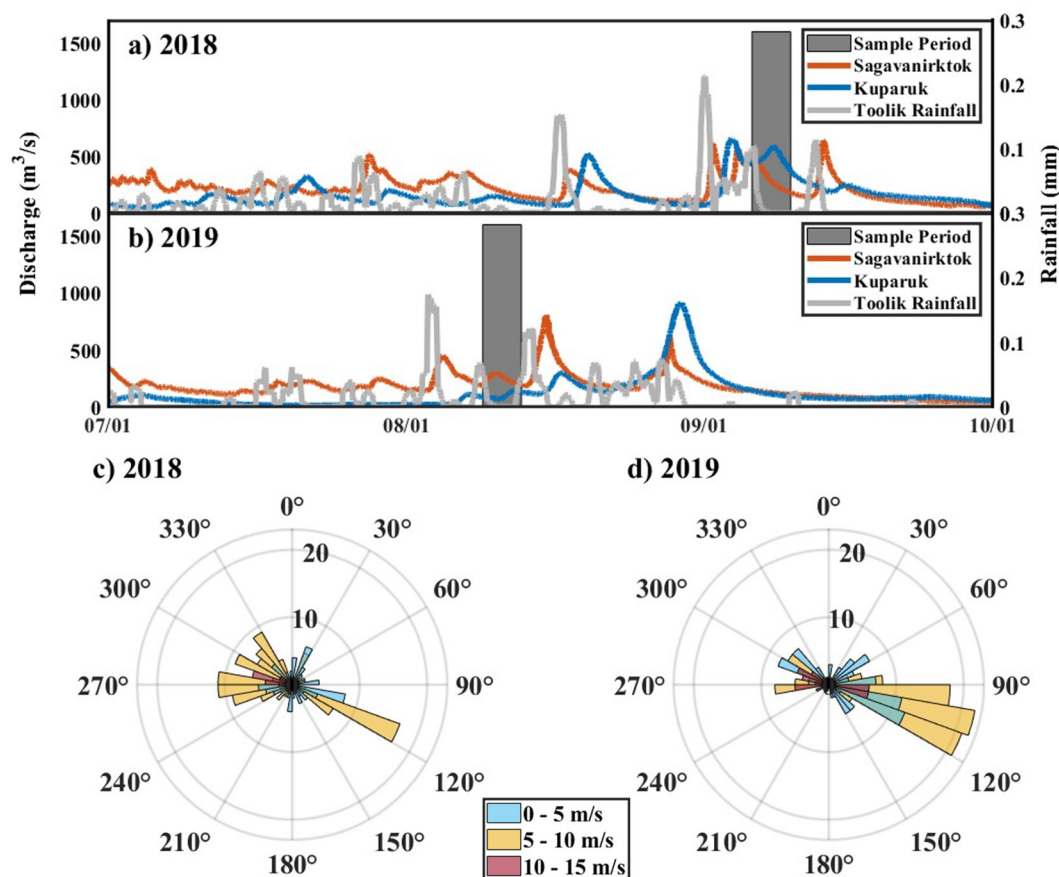


**Figure 6.** 2018 (a) and 2019 (b) volumetric flow measured at stations USGS 15896000 and USGS 15908000 for the Kugaruk and Sagavanirktok, respectively. Rainfall data were measured at Toolik Field Station and are presented as a 24-hr running mean (EDCT, 2020). Our field studies occurred between 6–10 September 2018 and 9–13 August 2019 (shaded areas). The lower panel shows wind direction histograms during 1–10 September 2018 (c) and 4–13 August 2019 (d). Radial values depict hourly wind readings in a given direction, polar values depict wind direction, and colors indicate wind speed.

The analyses in this study improve our understanding of the biogeochemistry of coastal Arctic margins that receive riverine input throughout the ice-free summer, in three ways. First, these analyses examine analytical measurements of DOC and POC along with their corresponding in situ optical characteristics during two summers characterized by different environmental forcing in this region. September 2018 was characterized by increased precipitation, persistent westerly winds (Figures 6c and 6d), and lingering sea ice in late summer, whereas August 2019 was much warmer than average in the months prior to sampling. Interannual variability can be expected in any coastal system, yet these 2018–2019 observational data provide valuable insight into distinctly different forcing climate phenomena that affect coastal organic carbon loads. Second, this study identified specific significant correlations between optical properties in Stefansson Sound and the concentration of DOC and POC. These optical properties may therefore represent proxies for the distribution and concentration of DOC and POC that can be implemented in autonomous systems to enable long-term in situ monitoring in difficult-to-access Arctic regions. Third, we found that across these 2 years, riverine discharge and wind-driven mixing jointly influenced the vertical and spatial distributions of temperature, salinity, and optical properties of organic matter within Stefansson Sound. Taken together, these findings provide valuable insight into how regional climate forcing phenomena such as precipitation and wind affect the vertical structure and areal character of biogeochemical and optical properties in coastal Arctic waters.

#### 4.1. Relationships Between Optical Properties and DOC and POC in Stefansson Sound

The primary findings in this study are the relationships between organic matter and optical properties of seawater: with DOC and fDOM,  $a_g(440)$ , and  $S_{412-550}$ , and with POC and optical backscatter at light wavelengths 470, 532,

and 660 nm. The strongest relationships for optical proxies across both years were seen between fDOM and DOC ( $r^2 = 0.67$ ) and  $b_p(470)$  and POC ( $r^2 = 0.90$ ). The weaker relationships were between  $a_g(440)$  and DOC in 2019 ( $r^2 < 0.001$ ) and  $b_p(660)$  and POC ( $r^2 = 0.59$ ) using data from 2018 to 2019. DOC and fDOM were well correlated in 2018 ( $r^2 = 0.94$ ) but not as well in 2019 ( $r^2 = 0.29$ ), which we ascribe to differences in the source and thus composition of the bulk DOC pool between the two years. For example, DOC derived from differing sources may contain fluorophores that do not fluoresce at the excitation wavelength of the fluorometer used in this study.

This fluorometer (WETLabs FLBBBCD) was configured with an excitation–emission pair close to Coble peak C (ex = 350 nm/em = 420–480 nm) which is indicative of the presence of lignin phenols and terrestrial humic materials (Coble, 1996; Walker et al., 2013). The fluorophores associated with these molecular assemblages are commonly found in high-latitude riverine discharge (Walker et al., 2013). Interestingly, in 2019, we observed fDOM concentrations between 2 and 14 ppm across all stations, without any statistically significant corresponding change in DOC concentration. This suggests that the DOC concentrations measured in 2019 may have represented organic matter with dynamic proportions of specific fluorophores. Moreover, peak A (ex = 260 nm/em = 380–460 nm) is also commonly found in the source waters of this region (Ward & Cory, 2015) and represents a fluorescent pool within the bulk DOC that would not be detected by the commonly used commercial DOM fluorometer we employed in our field study. Allochthonous marine humic material, indicated by peak M (ex = 312 nm/em = 380–420 nm) and also often observed in coastal Arctic waters (Drozdova et al., 2022), may similarly be a portion of the DOC pool captured in our analytically measured DOC concentrations but spectrally invisible to the fluorometer used in this study.

These nuances aside, the optical relationships presented here can be considered reasonably accurate proxies for estimating DOC in these coastal Arctic waters (MdAPD = ~25%). These relationships provide a means to observe DOC variability in these coastal regions with high temporal resolution, for example, by using in situ sensors mounted on autonomous platforms. Such fluorometers have already been used on autonomous sampling platforms in the coastal Arctic to obtain high temporal resolution observations of ephemeral events like the spring freshet (Laney & Okkonen, 2022). However, our in-depth examination of these optical relationships suggests that considerably more can be learned from using combinations of fluorometers assigned to measure all fluorophores expected in the coastal Arctic DOM pool. For example, a pair of fluorometers separately measuring both the A and M Coble peaks could be used specifically to better track changes in the relative abundance of allochthonous organic material versus that of terrestrial origin.

The absorption coefficient of solutes at 350 nm is a commonly used proxy for approximating DOC concentration, specifically lignin components due to the high concentration of aromatic and conjugated material that absorbs heavily in the UV within bulk DOM pools (Mann et al., 2016; Spencer et al., 2012; Weishaar et al., 2003). For visible wavelengths, the relationship between riverine DOC and the absorption coefficient of blue light is also strong across pan-Arctic rivers, including the nearby Hulahula and Jago Rivers on the Alaskan North Slope (Novak et al., 2022). In our in situ spectral absorption profiles, we observed a similarly strong relationship between DOC and absorption of 440 nm light ( $r^2 = 0.95$ ) in 2018. In 2019, however the correlation was poor ( $r^2 < 0.001$ ), which may potentially be due to instrument artifact such as a failure in the filter system that allowed large particles (greater than 0.2  $\mu\text{m}$  in diameter) into the measurement tube, or alternatively increased presence of small mineral particles that enhanced scattering errors in our absorption measurements. Such measurement artifacts could explain why values of  $a_g(440)$  increase for some stations in 2019 despite concentrations of DOC being similar (Figure 2b).

Typical analyses of the spectral slope of the absorption coefficient of solutes use spectral ranges between 275–295 and 350–400 nm because of their direct correlation with molecular weight (Helms et al., 2008). This makes spectral slopes in these wavelengths an effective proxy for tracing terrigenous dissolved organic matter in river-fed coastal margins (Fichot & Benner, 2012). Our in situ spectrophotometer does not include these ultraviolet wavelengths, unfortunately, but in the visible wavelengths, we found that the spectral slope from 412 to 550 nm correlated well to DOC concentration ( $r^2 = 0.70$ ) across both years of our study. We observed a steepening in spectral slope with increasing DOC concentrations, but it is not clear what this observation indicates. One possible explanation may relate to the molecular weight of the organic material. Spectral slope is expected to increase during photodegradation as larger molecules are degraded to smaller molecules (Twardowski & Donaghay, 2002). Smaller humic molecules also tend to fluoresce more than larger ones (Hayase & Tsubota, 1985). Consequently, the positive relationships we found between both spectral slope and fluorescence, and DOC concentration, could

indicate that in Stefansson Sound, increasing levels of DOC during late summer correspond to concentrations with proportionally smaller molecular compositions due to increased cumulative photobleaching.

In both years in Stefansson Sound, the backscattering coefficient at 470, 532, and 660 nm was well correlated with POC ( $r^2 = 0.90, 0.71, \text{ and } 0.59$ , respectively). The slope and intercept of the POC and backscatter relationship are very similar between 470 nm (blue) and 532 nm (green), suggesting that these particulate assemblages backscatter light at 470 and 532 nm to a nearly equal extent. The instrument we used in our study to measure backscatter has a lower saturation limit with its  $b_b(532)$  channel compared to its  $b_b(470)$  channel. This limits this instrument's utility for estimating POC concentration in environments with high concentrations of particulates. It also likely explains why the correlation between POC and  $b_b(470)$  is better when comparing these two wavelengths. The relatively poor correlation with backscatter at 660 nm may be instrument and/or statistical artifact, as these measurements most often reached the instrument's saturation limit and thus provided the smallest sample size. Other statistical approaches for estimating POC from optical backscatter show a lesser difference between  $b_b(470)$  and  $b_b(660)$  (e.g., MdAPD of 25.2% vs. 28.9%). Interestingly, excluding the data pairs displaying saturation in the red channel, from the  $b_b(470)$  regression, substantially weakens the relationship between  $b_b(470)$  and POC concentration ( $r^2 = 0.54$ , MdAPD = 29.8%), suggesting that the large range of  $b_b(470)$  values contributes to the goodness of fit.

One important consequence of the above analyses is that there are substantial limitations to estimating POC from backscatter by particles alone, especially across environments where the characteristics of suspended particulate matter may vary. Our observations encompass a fairly homogenous assemblage of particulate materials, and our observed relationships appear fairly robust. Yet the large variations in the relationship between POC and backscatter reported by other researchers underscore the critical importance of understanding particle composition when deriving such relationships (Koestner et al., 2022; Reynolds et al., 2016; Stramski et al., 1999). Some mineral-dominated samples exhibit strong correlations between POC and optical backscatter, but organic-dominated particle assemblages deviate greatly from said trends. While most of the particulates from Stefansson Sound fall in the mineral-dominated category (Koestner et al., 2021), it is possible that during periods of high riverine discharge such as the spring freshet, the bulk composition shifts more toward organic particulate matter, with both POC and PON becoming elevated during such an event (McClelland et al., 2014).

#### 4.2. Physical Controls on Distributions of Organic Matter Within Stefansson Sound

Our observations suggest that the vertical structure of water column properties within Stefansson Sound can be influenced strongly by the wind direction, by riverine discharge, and by distance to any nearby river mouth. Westerly downwelling-favorable winds push water against the coast and cause the river plume to remain closely trapped along coast toward the east. Easterly upwelling-favorable winds promote seaward advection of the river plume and facilitate wind-driven mixing in the water column (García Berdeal et al., 2002). In 2018, prevailing winds blew from the west, whereas in 2019 prevailing winds tended to blow from the east (Figures 6c and 6d). These Ekman dynamics are partially responsible for the areal distribution of river plume water within Stefansson Sound and thus play a large role in influencing surface temperature, salinity, DOC, and POC characteristics at any given station.

Westerly winds and relatively high recent precipitation in the adjacent watershed create multiple density strata in Stefansson Sound water columns. Measured densities ranged from  $1,002 \text{ kg m}^{-3}$  at the surface to  $1,025 \text{ kg m}^{-3}$  at depths of 5 m and below. These strata typically included a freshwater lens at the top, a mixed layer in the middle, and an oceanic layer near the bottom. In 2018, the stations furthest west (K1 and S1) exhibited thinner surface layers overlying slightly more dense oceanic waters, indicating strong stratification. Eastern stations (N1 and KAD1) were more weakly stratified albeit with thicker and substantially fresher surface lenses. The freshwater lenses at these eastern stations are likely due to their proximity to the nearby river mouths, whereas the western stations are further from river sources and overlying freshwater plumes have more opportunity to mix with oceanic waters below. Additionally, 2018 was characterized by weak westerly winds such that most mixing of the river plume was buoyancy driven, not wind driven. This is also apparent in the optical profiles where backscatter at N1 and KAD1 shows stronger surface signals than at K1 and S1, which being further from the rivers have surface waters that experienced longer periods to arrive at these sites, and thus more opportunity for particulates to settle out of the surface plume (Figure 4). In contrast, density profiles in 2019 indicated more saline and well-mixed water columns throughout Stefansson Sound. The western stations (K1, KS1, and S1) exhibited a thin, fresh surface layer overlying a predominantly oceanic bottom layer. As with 2018, this is likely due to their proximity to the river mouths which constantly inject some amount of freshwater throughout

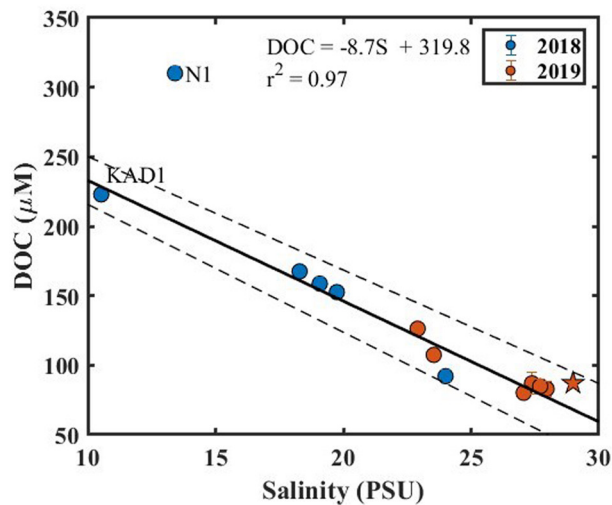


**Figure 7.** Relationship between surface dissolved organic carbon (DOC) concentration and salinity within Stefansson Sound over both years. Dotted lines indicate  $\pm 1$  SD. Star symbol indicates the marine end member station (UPE80 2019). All samples are included in this regression except N1 2018.

the summer regardless of rainfall over the adjacent watersheds. The more offshore stations (S2 and UPE80) exhibited deeper mixed layers starting at  $\sim 8$  m at S2 and  $\sim 19$  m at UPE80.

Given this continuous supply of riverine freshwater, rivers can be expected to be a primary source of organic matter to this coastal system in summer, but sea ice is also intermittently present in Stefansson Sound in late summer in certain years. Over both 2018 and 2019, DOC concentration decreased with increasing salinity ( $r^2 = 0.97$ ) throughout Stefansson Sound, confirming that DOC in these waters is associated with freshwater inputs. We noted that the relationship between DOC concentrations and salinity appears to be anomalously high at station N1 in 2018. Omitting this station from our regression reveals a strong linear correlation with  $r^2$  of 0.97 (Figure 7). This anomaly could reflect contamination during sampling, or DOC levels at N1 that year could in fact have been anomalously high with respect to the seemingly linear trend with salinity. We note that removing not just N1 but also the data point representing our lowest salinity sample (from station KAD1 2018, extremely close to shore in the mouth of the Kadleroshilik River) still presents a strong linear correlation with an  $r^2$  of 0.94 and a slightly different relationship of  $-9.2 \mu\text{mol PSU}^{-1}$ . If we exclude the N1 observations and extrapolate the linear model to zero salinity, we would infer that the freshwater sources to Stefansson Sound contain a DOC concentration of  $320 \mu\text{M}$ .

If we instead retain the sample at N1 and treat the KAD1 sample as anomalous, the remaining data also can be well represented using an exponential nonlinear model ( $r^2 = 0.97$ ) with an intercept at 0 PSU of  $1,110 \mu\text{M}$ . A linear model that ignores our N1 data therefore suggests a value that falls in the middle of the  $100\text{--}600 \mu\text{M}$  range measured in the Sagavanirktok and Kuparuk Rivers by other workers during late summer (McClelland et al., 2014). Melting sea ice also is characterized by DOC concentrations in this range (Underwood et al., 2019). However, the model inclusive of N1 and exclusive of KAD1 suggests a value closer to that measured during spring freshets in the Kuparuk River (Holmes et al., 2008) as well as that estimated in groundwater runoff from nearby coastlines (Connolly et al., 2020). If conservative physical mixing is assumed to be the primary mechanism for distributing DOC within Stefansson Sound, there is no reason to invoke a nonlinear model. However, degradation pathways such as microbial respiration and photo-oxidation may remove DOC from the system independent of mixing, which would be nonconservative and therefore require a nonlinear model to describe. Resolving this will likely require further study of degradation pathways that can remove carbon from coastal Arctic lagoons.

Other aspects of our observations provide additional insight into the underlying drivers of these year-to-year differences in DOC concentrations in Stefansson Sound. In 2018, heavy rainfall in the adjacent watershed prior to our field sampling increased riverine discharge and likely contributed to the higher surface concentrations of DOC, compared to what was measured during 2019 (unpaired  $t$  test,  $p < 0.05$ ) during a period that was preceded by relatively lower rainfall. Also, sea ice in 2018 persisted in these coastal waters throughout the summer and into fall. During the 2018 field season, we encountered an ice floe at our K1 station, and we hypothesize that the ongoing melting of this floe and others nearby contributed the different temperature–salinity characteristics seen at this location compared to other stations within the same year (Figure 5), and also evident as a more complex vertical structure at K1, with multiple layers as seen in the density profiles (Figure 4). Notably, our DOC sample from K1 in 2018 was not taken from the surface freshwater lens itself but from an intermediate mixed layer immediately below. Our mixing model for salinity and DOC includes this 2018 K1 sample, which likely incorporates the influence of sea-ice melt and associated organic matter into the overall mixing model. Therefore, in future years when regional sea ice may occur with less frequency or is absent altogether, this mixing model would underestimate the anticipated concentration of organic matter associated with freshwater inputs. Additionally, climate change is accelerating groundwater discharge and permafrost thaw, which will provide a new source of organic material within the freshwater being delivered by rivers to these local coastal Arctic ecosystems (Connolly et al., 2020).

### 4.3. Implications for Satellite Remote Sensing of Arctic Coastal Waters

The in situ observations presented in this study offer insight into the optical character, spatial distributions, and annual variability of organic matter in this particular area along the Alaskan Arctic coast. As is typical with coastal Arctic systems, in situ insight is limited both spatially and temporally, and ocean color remote sensing might potentially help improve our understanding of organic matter sources and distributions in coastal Arctic regions. This study provides information about the interrelationships between absorption and backscatter by organic material in optically complex coastal waters, which may be valuable for improving quasi-analytical and inverse remote sensing algorithms for estimating quantities and qualities of organic matter in these waters. Current remote sensing approaches for assessing POC (Lee et al., 2002; Loisel & Stramski, 2000; Maritorena et al., 2002) and DOC (Mannino et al., 2008), including those developed for use in Arctic waters (Juhls et al., 2022; Matsuoka et al., 2013), can potentially benefit from such in situ observations along the coastal Arctic, to improve calibration and validation of ocean color algorithms for nearshore regions and especially regions that are adjacent to the smaller, less well studied Arctic rivers like the Sagavanirktok and Kuparuk that feed Stefansson Sound.

Our in situ observations also suggest a role for satellite remote sensing to better examine the finer-scale variability in DOC and POC that occurs spatially in such relatively small coastal embayments. Some of the variability in our optical data will be manifested in the remote sensing reflectance spectra measured by satellite platforms having relatively fine spatial resolutions, such as Landsat and Sentinel. These platforms can potentially further our ability to examine spatial distribution of organic matter in Stefansson Sound and other Alaskan lagoons and estuaries that are not as easily accessed for direct sampling. Additionally, sensors with finer spectral resolution, such as the Ocean Color Instrument (OCI) soon to be launched on NASA's PACE mission, offer possibilities to examine these optically complex coastal Arctic waters from a hyperspectral perspective. Hyperspectral approaches may eventually provide capability to assess the quality of organic matter via its absorption characteristics. With the OCI for example, its ability to sense remote sensing reflectance down to 300 nm may enable an adaptation of methods for assessing organic matter quality that leverage absorption in these UV wavelengths (Harringmeyer et al., 2021; Helms et al., 2008).

### 4.4. Future Directions

Findings from this field study provide several avenues for future research into the optical character and organic matter biogeochemistry of Arctic coastal margins. Importantly, our analyses suggest that standard optical proxies for DOC do not account for the entire amount we measured analytically in Stefansson Sound. To quantify the entire DOC pool in those waters or elsewhere in the coastal Arctic, there may be advantages to leveraging multiple fluorometers with different but appropriate excitation–emission pairs, that in concert can better detect the entire DOC pool. This approach might be particularly valuable when using autonomous platforms in coastal regions where organic material occurs with relatively high abundance in Coble peaks A and M. Fluorometers that assess these and other peaks in addition to the routine peak C could potentially better discriminate sources of DOC in addition to concentration. For example, the ratio of peak T (270/340 nm) to peak A is expected to reflect the relative contribution of protein fluorescence relative to that of terrestrially sourced humic material. Similarly, the ratio of peak M to peak C is expected to reflect the relative contribution of microbially derived to terrestrially sourced DOM (Stedmon & Cory, 2014). Further studies would help assess the robustness and utility of such simple applications of spectral fluorescence measurement for studying organic matter sources and distributions in coastal Arctic systems.

This study also revealed significant hydrographic and optical complexity in Stefansson Sound, suggesting that this small coastal embayment and the rivers that feed it are not necessarily well modeled as smaller versions of the better studied larger Arctic rivers such as the Yukon, Mackenzie, Kolyma, and Lena. In both years, discharge from local Alaskan rivers and regional winds played a large role in establishing surface water hydrography and spatial distributions of DOC and POC. However, in these 2 years, differences were apparent in the optical correlations with DOC and in the vertical structure of hydrographic and optical properties. These differences warrant caution when using data sets from any single study or any single year as representative, for describing coastal Arctic systems or for the purposes of developing autonomous sensing platforms to study organic matter dynamics in those regions.

This research highlights the importance of interdisciplinary approaches for understanding systems-level phenomena in Arctic coastal margins. Coastal systems in the Arctic experience complex environmental forcing not seen

at lower latitudes, such as the interplay between sea ice and strong riverine inputs during and after the spring freshet. Terrestrial inputs of organic matter are highly susceptible to larger-scale meteorological forcing and are strongly affected by coastal erosion that is widespread along Arctic coastal margins (Jones et al., 2009). The Arctic Ocean is experiencing unprecedented environmental changes, such as increased warming and precipitation (Bintanja & Andry, 2017). Its coastal margins are undergoing changes that in turn may alter their biogeochemistry and their role in the global carbon cycle. One notable change may be occurring in the timing and duration of the ice-free season, which may be extending further into the fall, which would substantially increase the total amount of organic matter delivered by these affected rivers (Bintanja & Selten, 2014). It is important to not extrapolate findings like ours too broadly to the entire pan-Arctic margin, though, given that certain phenomena such as spring freshet, which appears to be occurring later in the season in North American Arctic watersheds, may exhibit the opposite trends in Eurasian watersheds (Feng et al., 2021).

Finally, although this study examines potential sources of organic material in Stefansson Sound, it does not address the potential fates of this material. Processes that degrade and utilize organic matter include photo-oxidation and microbial respiration, the latter of which is dependent on the quality of the organic material provided by riverine and sea-ice sources. Much of the material transported by the rivers is either fully degraded or partially degraded by photo-oxidation and mineralization before it reaches the coastal margin (Cory et al., 2014; Kaiser et al., 2017). This process breaks high-molecular-weight molecules down into lower-molecular-weight molecules. This phenomenon could explain the positive relationship between  $S_{412-550}$  and DOC noted in this study, which suggests that higher DOC concentrations contain larger proportions of low molecular weight molecules. Interestingly, it has been shown that recently thawed permafrost carbon and carbon found far downstream in Arctic Alaskan rivers are both highly bioavailable (Holmes et al., 2008; Vonk et al., 2013). However, it is unclear to what degree this riverine or ice-originating carbon is eventually bioavailable after it is resident for some time in such shallow Arctic coastal lagoons. It is also unclear how the spectral fluorescence characteristics of this organic carbon might change due to any degradation processes that occur in coastal waters. Future studies could potentially fill this knowledge gap by examining the organic matter conversion to carbon dioxide in dark and light incubations of river water versus coastal water, while concurrently monitoring changes in spectral absorption and fluorescence. This would provide valuable information to better understand the nature and fates of organic material in coastal Arctic systems, specifically with respect to its role in and contribution to local biogeochemical cycles.

## Data Availability Statement

Data from this project are stored on NASA's SeaBass public access database under the experiment Prudhoe\_Freshets. DOI for access to these data is 10.5067/SeaBASS/PRUDHOE\_FRESHETS/DATA001; [https://seabass.gsfc.nasa.gov/experiment/Prudhoe\\_Freshets](https://seabass.gsfc.nasa.gov/experiment/Prudhoe_Freshets).

## Acknowledgments

This research was funded by the National Aeronautics and Space Administration's Carbon Cycle and Ecosystems (CCE) program (award NNX17AI72G), and field work was conducted under permit from Alaska's North Slope Borough (DPCS #18-433). We thank British Petroleum Exploration Alaska for facilitating access to our field sites. We give special thanks to Captain Mike Fleming (*R/V Ukpik*) for his expertise and guidance during our open water field seasons. We thank Gretchen Swarr for help in cruise preparation and sample analysis and Dariusz Stramski for valuable comments and expertise with our particle optics analyses. Finally, we thank our two anonymous reviewers who provided careful and thoughtful reviews of this manuscript.

## References

- Belzile, C., Johannessen, S. C., Gosselin, M., Demers, S., & Miller, W. L. (2000). Ultraviolet attenuation by dissolved and particulate constituents of first-year ice during late spring in an Arctic polynya. *Limnology & Oceanography*, 45(6), 1265–1273. <https://doi.org/10.4319/lo.2000.45.6.1265>
- Bintanja, R., & Andry, O. (2017). Towards a rain-dominated Arctic. *Nature Climate Change*, 7(4), 263–267. <https://doi.org/10.1038/nclimate3240>
- Bintanja, R., & Selten, F. M. (2014). Future increases in Arctic precipitation linked to local evaporation and sea-ice retreat. *Nature*, 509(7501), 479–482. <https://doi.org/10.1038/nature13259>
- Chang, G. C., & Dickey, T. D. (2001). Optical and physical variability on timescales from minutes to the seasonal cycle on the New England shelf: July 1996 to June 1997. *Journal of Geophysical Research*, 106(C5), 9435–9453. <https://doi.org/10.1029/2000JC900069>
- Coble, P. G. (1996). Characterization of marine and terrestrial DOM in seawater using excitation–emission matrix spectroscopy. *Marine Chemistry*, 51(4), 325–346. [https://doi.org/10.1016/0304-4203\(95\)00062-3](https://doi.org/10.1016/0304-4203(95)00062-3)
- Connolly, C. T., Cardenas, M. B., Burkart, G. A., Spencer, R. G. M., & McClelland, J. W. (2020). Groundwater as a major source of dissolved organic matter to Arctic coastal waters. *Nature Communications*, 11(1), 1479. <https://doi.org/10.1038/s41467-020-15250-8>
- Connolly, C. T., Khosh, M. S., Burkart, G. A., Douglas, T. A., Holmes, R. M., Jacobson, A. D., et al. (2018). Watershed slope as a predictor of fluvial dissolved organic matter and nitrate concentrations across geographical space and catchment size in the Arctic. *Environmental Research Letters*, 13(10), 104015. <https://doi.org/10.1088/1748-9326/aae35d>
- Cory, R. M., Ward, C. P., Crump, B. C., & Kling, G. W. (2014). Sunlight controls water column processing of carbon in arctic fresh waters. *Science*, 345(6199), 925–928. <https://doi.org/10.1126/science.1253119>
- Drozдова, A. N., Krylov, I. N., Nedospasov, A. A., Arashkevich, E. G., & Labutin, T. A. (2022). Fluorescent signatures of autochthonous dissolved organic matter production in Siberian shelf seas. *Frontiers in Marine Science*, 9, 872557. <https://doi.org/10.3389/fmars.2022.872557>
- EDCT. (2020). Meteorological monitoring program at Toolik. Retrieved from <https://toolik.alaska.edu/edc/monitoring/abiotic/met-data-query.php>
- Feng, D., Gleason, C. J., Lin, P., Yang, X., Pan, M., & Ishitsuka, Y. (2021). Recent changes to Arctic river discharge. *Nature Communications*, 12(1), 6917. <https://doi.org/10.1038/s41467-021-27228-1>

- Fichot, C. G., & Benner, R. (2012). The spectral slope coefficient of chromophoric dissolved organic matter (S<sub>275–295</sub>) as a tracer of terrigenous dissolved organic carbon in river-influenced ocean margins. *Limnology & Oceanography*, *57*(5), 1453–1466. <https://doi.org/10.4319/lo.2012.57.5.1453>
- García Berdeal, I., Hickey, B. M., & Kawase, M. (2002). Influence of wind stress and ambient flow on a high discharge river plume. *Journal of Geophysical Research*, *107*(C9), 3130. <https://doi.org/10.1029/2001JC000932>
- Gonçalves-Araujo, R., Granskog, M. A., Bracher, A., Azetsu-Scott, K., Dodd, P. A., & Stedmon, C. A. (2016). Using fluorescent dissolved organic matter to trace and distinguish the origin of Arctic surface waters. *Scientific Reports*, *6*(1), 33978. <https://doi.org/10.1038/srep33978>
- Harringmeyer, J. P., Kaiser, K., Thompson, D. R., Gierach, M. M., Cash, C. L., & Fichot, C. G. (2021). Detection and sourcing of CDOM in urban coastal waters with UV-visible imaging spectroscopy. *Frontiers in Environmental Science*, *9*, 647966. <https://doi.org/10.3389/fenvs.2021.647966>
- Hayase, K., & Tsubota, H. (1985). Sedimentary humic acid and fulvic acid as fluorescent organic materials. *Geochimica et Cosmochimica Acta*, *49*(1), 159–163. [https://doi.org/10.1016/0016-7037\(85\)90200-5](https://doi.org/10.1016/0016-7037(85)90200-5)
- Helms, J. R., Stubbins, A., Ritchie, J. D., Minor, E. C., Kieber, D. J., & Mopper, K. (2008). Absorption spectral slopes and slope ratios as indicators of molecular weight, source, and photobleaching of chromophoric dissolved organic matter. *Limnology & Oceanography*, *53*(3), 955–969. <https://doi.org/10.4319/lo.2008.53.3.0955>
- Holmes, R. M., McClelland, J. W., Raymond, P. A., Frazer, B. B., Peterson, B. J., & Stieglitz, M. (2008). Lability of DOC transported by Alaskan rivers to the Arctic Ocean. *Geophysical Research Letters*, *35*, L03402. <https://doi.org/10.1029/2007GL032837>
- Howell, S., Brady, M., Derksen, C., & Kelly, R. (2016). Recent changes in sea ice area flux through the Beaufort Sea during the summer. *Journal of Geophysical Research: Oceans*, *121*, 2659–2672. <https://doi.org/10.1002/2015JC011464>
- Jones, B. M., Arp, C. D., Jorgenson, M. T., Hinkel, K. M., Schmutz, J. A., & Flint, P. L. (2009). Increase in the rate and uniformity of coastline erosion in Arctic Alaska. *Geophysical Research Letters*, *36*, L03503. <https://doi.org/10.1029/2008GL036205>
- Juhls, B., Matsuoka, A., Lizotte, M., Bécu, G., Overduin, P. P., El Kassar, J., et al. (2022). Seasonal dynamics of dissolved organic matter in the Mackenzie Delta, Canadian Arctic waters: Implications for ocean colour remote sensing. *Remote Sensing of Environment*, *283*, 113327. <https://doi.org/10.1016/j.rse.2022.113327>
- Kaiser, K., Canedo-Oropeza, M., McMahon, R., & Amon, R. M. W. (2017). Origins and transformations of dissolved organic matter in large Arctic rivers. *Scientific Reports*, *7*(1), 13064. <https://doi.org/10.1038/s41598-017-12729-1>
- Klein, K. P., Lantuit, H., Heim, B., Doxaran, D., Juhls, B., Nitze, I., et al. (2021). The Arctic Nearshore Turbidity Algorithm (ANTA)—A multi sensor turbidity algorithm for Arctic nearshore environments. *Science of Remote Sensing*, *4*, 100036. <https://doi.org/10.1016/j.srs.2021.100036>
- Koestner, D., Stramski, D., & Reynolds, R. A. (2021). Characterization of suspended particulate matter in contrasting coastal marine environments with angle-resolved polarized light scattering measurements. *Applied Optics*, *60*(36), 11161–11179. <https://doi.org/10.1364/AO.441226>
- Koestner, D., Stramski, D., & Reynolds, R. A. (2022). A multivariable empirical algorithm for estimating particulate organic carbon concentration in marine environments from optical backscattering and chlorophyll-*a* measurements. *Frontiers in Marine Science*, *9*, 941950. <https://doi.org/10.3389/fmars.2022.941950>
- Laney, S. R., & Okkonen, S. (2022). An autonomous buoy system for observing spring freshet plumes under landfast sea ice. *Limnology and Oceanography: Methods*, *20*(1), 15–25. <https://doi.org/10.1002/lom3.10472>
- Lee, Z., Carder, K. L., & Arnone, R. A. (2002). Deriving inherent optical properties from water color: A multiband quasi-analytical algorithm for optically deep waters. *Applied Optics*, *41*(27), 5755–5772. <https://doi.org/10.1364/AO.41.005755>
- Loisel, H., & Stramski, D. (2000). Estimation of the inherent optical properties of natural waters from the irradiance attenuation coefficient and reflectance in the presence of Raman scattering. *Applied Optics*, *39*(18), 3001–3011. <https://doi.org/10.1364/AO.39.003001>
- Mann, P. J., Spencer, R. G. M., Hernes, P. J., Six, J., Aiken, G. R., Tank, S. E., et al. (2016). Pan-Arctic trends in terrestrial dissolved organic matter from optical measurements. *Frontiers of Earth Science*, *4*, 25. <https://doi.org/10.3389/feart.2016.00025>
- Mannino, A., Russ, M. E., & Hooker, S. B. (2008). Algorithm development and validation for satellite-derived distributions of DOC and CDOM in the U.S. Middle Atlantic Bight. *Journal of Geophysical Research*, *113*, C07051. <https://doi.org/10.1029/2007JC004493>
- Maritorena, S., Siegel, D. A., & Peterson, A. R. (2002). Optimization of a semi-analytical ocean color model for global-scale applications. *Applied Optics*, *41*(15), 2705–2714. <https://doi.org/10.1364/AO.41.002705>
- Matsuoka, A., Bricaud, A., Benner, R., Para, J., Sempéré, R., Prieur, L., et al. (2012). Tracing the transport of colored dissolved organic matter in water masses of the southern Beaufort Sea: Relationship with hydrographic characteristics. *Biogeosciences*, *9*(3), 925–940. <https://doi.org/10.5194/bg-9-925-2012>
- Matsuoka, A., Hill, V., Huot, Y., Babin, M., & Bricaud, A. (2011). Seasonal variability in the light absorption properties of western Arctic waters: Parameterization of the individual components of absorption for ocean color applications. *Journal of Geophysical Research*, *116*, C02007. <https://doi.org/10.1029/2009JC005594>
- Matsuoka, A., Hooker, S. B., Bricaud, A., Gentili, B., & Babin, M. (2013). Estimating absorption coefficients of colored dissolved organic matter (CDOM) using a semi-analytical algorithm for southern Beaufort Sea waters: Application to deriving concentrations of dissolved organic carbon from space. *Biogeosciences*, *10*(2), 917–927. <https://doi.org/10.5194/bg-10-917-2013>
- McClelland, J. W., Holmes, R. M., Peterson, B. J., Raymond, P. A., Striegl, R. G., Zhulidov, A. V., et al. (2016). Particulate organic carbon and nitrogen export from major Arctic rivers. *Global Biogeochemical Cycles*, *30*, 629–643. <https://doi.org/10.1002/2015GB005351>
- McClelland, J. W., Townsend-Small, A., Holmes, R. M., Pan, F., Stieglitz, M., Khosh, M., & Peterson, B. J. (2014). River export of nutrients and organic matter from the North Slope of Alaska to the Beaufort Sea. *Water Resources Research*, *50*, 1823–1839. <https://doi.org/10.1002/2013WR014722>
- Novak, M. G., Cetinić, I., Chaves, J. E., & Mannino, A. (2018). The adsorption of dissolved organic carbon onto glass fiber filters and its effect on the measurement of particulate organic carbon: A laboratory and modeling exercise. *Limnology and Oceanography: Methods*, *16*(6), 356–366. <https://doi.org/10.1002/lom3.10248>
- Novak, M. G., Mannino, A., Clark, J. B., Hernes, P., Tzortziou, M., Spencer, R. G. M., et al. (2022). Arctic biogeochemical and optical properties of dissolved organic matter across river to sea gradients. *Frontiers in Marine Science*, *9*, 949034. <https://doi.org/10.3389/fmars.2022.949034>
- Osburn, C. L., Boyd, T. J., Montgomery, M. T., Bianchi, T. S., Coffin, R. B., & Paerl, H. W. (2016). Optical proxies for terrestrial dissolved organic matter in estuaries and coastal waters. *Frontiers in Marine Science*, *2*, 127. <https://doi.org/10.3389/fmars.2015.00127>
- Parsons, T. R., Maita, Y., & Lalli, C. M. (1984). A manual of chemical and biological methods for seawater analysis. Retrieved from <https://www.cambridge.org/core/article/t-r-parsons-y-maita-c-m-lalli-1984-a-manual-of-chemical-and-biological-methods-for-seawater-analysis-xiv-173-pp-oxford-pergamon-press-price-550-us-895-flexicover-isbn-0-08-030288-2-hard-cover-0-08-030287-4-flexicover/D6B472FF1C39AD26EFB9085425EE57E5>
- Petzold, T. J. (1972). *Volume scattering functions for selected ocean waters*. Scripps Institution of Oceanography, UC San Diego. Retrieved from <https://escholarship.org/uc/item/73p3r43q>

- Reynolds, R. A., Stramski, D., & Neukermans, G. (2016). Optical backscattering by particles in Arctic seawater and relationships to particle mass concentration, size distribution, and bulk composition. *Limnology & Oceanography*, *61*(5), 1869–1890. <https://doi.org/10.1002/lno.10341>
- Spencer, R. G. M., Butler, K. D., & Aiken, G. R. (2012). Dissolved organic carbon and chromophoric dissolved organic matter properties of rivers in the USA. *Journal of Geophysical Research*, *117*, G03001. <https://doi.org/10.1029/2011JG001928>
- Stedmon, C. A., Amon, R. M. W., Rinehart, A. J., & Walker, S. A. (2011). The supply and characteristics of colored dissolved organic matter (CDOM) in the Arctic Ocean: Pan arctic trends and differences. *Marine Chemistry*, *124*(1), 108–118. <https://doi.org/10.1016/j.marchem.2010.12.007>
- Stedmon, C. A., & Cory, R. M. (2014). Biological origins and fate of fluorescent dissolved organic matter. In *Aquatic organic matter fluorescence*. Stramski, D., Reynolds, R. A., Kahru, M., & Mitchell, B. G. (1999). Estimation of particulate organic carbon in the ocean from satellite remote sensing. *Science*, *285*(5425), 239–242. <https://doi.org/10.1126/science.285.5425.239>
- Sullivan, J. M., Twardowski, M. S., Zaneveld, J. R. V., Moore, C. M., Barnard, A. H., Donaghay, P. L., & Rhoades, B. (2006). Hyperspectral temperature and salt dependencies of absorption by water and heavy water in the 400–750 nm spectral range. *Applied Optics*, *45*(21), 5294–5309. <https://doi.org/10.1364/AO.45.005294>
- Twardowski, M. S., & Donaghay, P. L. (2002). Photobleaching of aquatic dissolved materials: Absorption removal, spectral alteration, and their interrelationship. *Journal of Geophysical Research*, *107*(C8), 3091. <https://doi.org/10.1029/1999JC000281>
- Underwood, G. J. C., Michel, C., Meisterhans, G., Niemi, A., Belzile, C., Witt, M., et al. (2019). Organic matter from Arctic sea-ice loss alters bacterial community structure and function. *Nature Climate Change*, *9*(2), 170–176. <https://doi.org/10.1038/s41558-018-0391-7>
- Vonk, J. E., Mann, P. J., Davydov, S., Davydova, A., Spencer, R. G. M., Schade, J., et al. (2013). High biolability of ancient permafrost carbon upon thaw. *Geophysical Research Letters*, *40*, 2689–2693. <https://doi.org/10.1002/grl.50348>
- Walker, S. A., Amon, R. M. W., & Stedmon, C. A. (2013). Variations in high-latitude riverine fluorescent dissolved organic matter: A comparison of large arctic rivers. *Journal of Geophysical Research: Biogeosciences*, *118*, 1689–1702. <https://doi.org/10.1002/2013JG002320>
- Ward, C. P., & Cory, R. M. (2015). Chemical composition of dissolved organic matter draining permafrost soils. *Geochimica et Cosmochimica Acta*, *167*, 63–79. <https://doi.org/10.1016/j.gca.2015.07.001>
- Weingartner, T., & Okkonen, S. R. (2001). Beaufort Sea nearshore under-ice currents: Science, analysis and logistics.
- Weishaar, J. L., Aiken, G. R., Bergamaschi, B. A., Fram, M. S., Fujii, R., & Mopper, K. (2003). Evaluation of specific ultraviolet absorbance as an indicator of the chemical composition and reactivity of dissolved organic carbon. *Environmental Science & Technology*, *37*(20), 4702–4708. <https://doi.org/10.1021/es030360x>
- Youcha, E. K., Gieck, R. E., Arp, C. D., Stuefer, S., & Irving, K. (2015). Standard operating procedure and workplan for the Terrestrial Environmental Observation Network (TEON)—Arctic landscape conservation cooperative: Kuparuk River basin and adjacent catchments. Retrieved from <http://hdl.handle.net/11122/10389>